YIELD STRESS ANOMALY IN B2 FeAl

K. YOSHIMI*, S. HANADA* and M. H. YOO**
*Institute for Materials Research, Tohoku University, Sendai 980-77, Japan
**Metals and Ceramics Division, ORNL, Oak Ridge, TN 37831-6115, USA

ABSTRACT

Our studies on yield stress anomaly of B2 FeAl single crystals are reviewed in this paper. A positive temperature dependence of yield stress, so-called "yield stress anomaly", is observed in B2 FeAl in which excess vacancies are fully annealed out. Associated with the anomaly, characteristic asymmetry is found between tension and compression. While the strain-rate sensitivity is almost zero in the temperature range of the yield stress anomaly, the stress relaxation becomes significant with increasing temperature, indicating that a recovery process is thermally activated. It is ascertained by the two-surface trace analysis that slip transition from <111> direction at intermediate temperature to <100> at high temperature occurs around the peak temperature. Even at the peak temperature, in addition, operative slip vector for yielding is confirmed to be predominantly <111> by TEM. Also, it is observed that <111>-type superdislocations are frequently climb-dissociated in the temperature range of the anomaly. APB formation on {111} plane is energetically favorable, which is in agreement with the Flinn's calculation for the B2 superlattice that APB energy on {111} plane is lower than that on {110} plane. Such an anisotropy of APB energy would offer specific driving force for the climb dissociation on <111> superdislocations. On the basis of the observed results, the anomalous strengthening behavior of B2 FeAl single crystals is discussed.

MASTER

INTRODUCTION

A mild peak of temperature-dependent yield stress in B2 FeAl was first observed in the paper by Baker and Gaydosh [1] who dealt with Fe-37Al-2Ni. (Compositions are described in mole per cent throughout this paper.) Later, Guo, Sun, Tan, Li and Lai [2] found the anomalous peak around 773 K in polycrystalline Fe-40Al+B. Chang [3] also found a distinct peak in large-grained, directionally solidified Fe-40Al. After Guo et al. [2] and Chang [3], the unusual yield behavior has become one of the hottest topics in B2 FeAl. Recently, the yield stress peak has been reported by many research groups [4 - 8], and also some theoretical and experimental efforts have been devoted to understanding the anomalous phenomenon in B2 FeAl [9 - 15]. Because of difficulty in assessing the prominent dislocation microstructure, a physical source(s) has not been identified. Though β-CuZn and DO3 Fe3Al are well-known to exhibit the yield stress anomaly [16 - 21], the anomalous strengthening mechanism has not been established for these either. Therefore, basic understanding of yielding and deformation behavior in B2 FeAl is not only necessary for clarifying the physical source(s) of the yield stress anomaly in B2 FeAl, but also very significant for a general viewpoint of the yield stress anomaly in bcc-base intermetallic compounds, including β-CuZn and DO3 Fe3Al.

In the present paper, we review the yield stress anomaly of B2 FeAl, mainly our studies using single crystals. The observed yield stress anomaly of B2 FeAl will be discussed by comparing with those in β-CuZn and DO3 Fe3Al.

DISCLAIMER

Portions of this document may be illegible
in electronic image products. Images are
produced from the best available original
document.

MACROSCOPIC STRENGTH AND DEFORMATION FEATURE OF SINGLE CRYSTALS

Temperature-dependent phenomena

In single crystals, yield stress peaks can be observed clearly (Fig. 1). The onset temperatures (T_I) observed in our studies, where yield stress begins to increase with increasing temperature, lie between $0.37\ T_c$ $(0.35\ T_m)$ and $0.44\ T_c$ $(0.41\ T_m)$, and the peak temperatures (T_p) lie between $0.51\ T_c$ $(0.47\ T_m)$ and $0.59\ T_c$ $(0.55\ T_m)$ near 40 Al [11, 12], where T_c is the B2/A2 transformation temperature and T_m the melting point from the phase diagram [22]. In stress-strain curves (Fig. 2), work hardening rate gradually decreases with increasing temperature up to T_p. Also, for some orientations, serrations appear above room temperature. Around T_p, serrations disappear over the whole strain range and instead a large yield drop takes place for all the orientations examined.

Figure 3 shows stress-strain curves of single crystals under higher magnification,
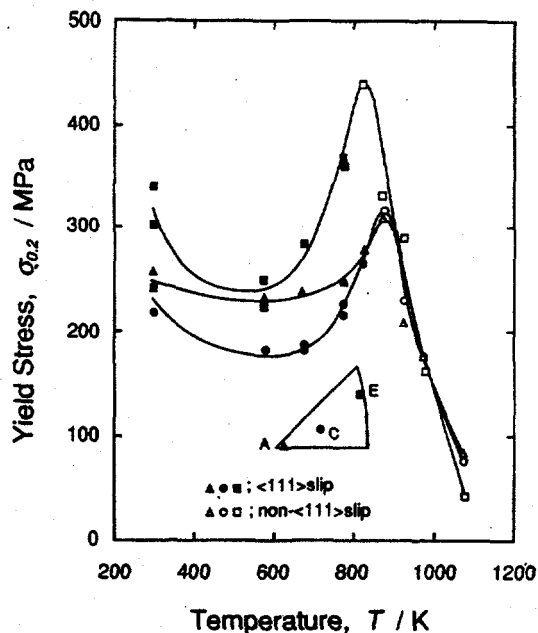
Fig. 1. Temperature and orientation dependence of yield stress of Fe-39.5Al single crystals [11]. Filled and open symbols indicate yield stress for [111] and non-[111] slip.
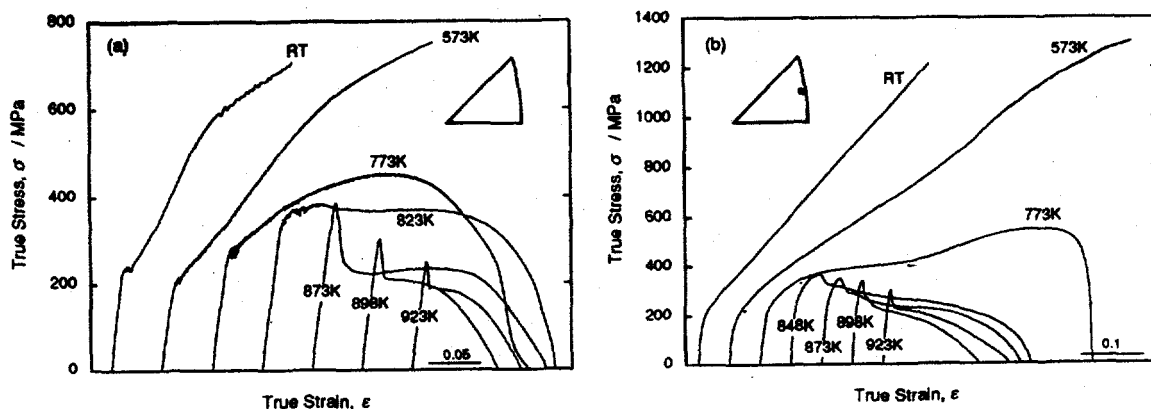
which were obtained during the stress relaxation tests in compression. Below T_p (Fig. 3(a)), the stress amplitude of serrations increases with increasing temperature. Similar results had been already observed in polycrystalline Fe-43Al by Morris et al. [23]. The increment in flow stress after the stress relaxation is almost zero below T_p; i.e., static strain aging (SSA) in this temperature range ($<T_p$) is not detectable in the crystal. Therefore, the serrations may not be due to dynamic strain aging (DSA) by solute atom atmospheres. At and just above T_p (823 K or 873 K), single crystals exhibit a minimum of flow stress (σ_m) after yield drops with no serration (Fig. 3(b)). Slight increases in stress after the stress relaxation can be also noted. Stress gap, $\Delta\sigma_y$, between the peak stress after yielding, σ_p, and σ_m is much larger than the stress increments after

Fig. 2. Stress-strain curves of Fe-39Al single crystals obtained by tensile tests [12].
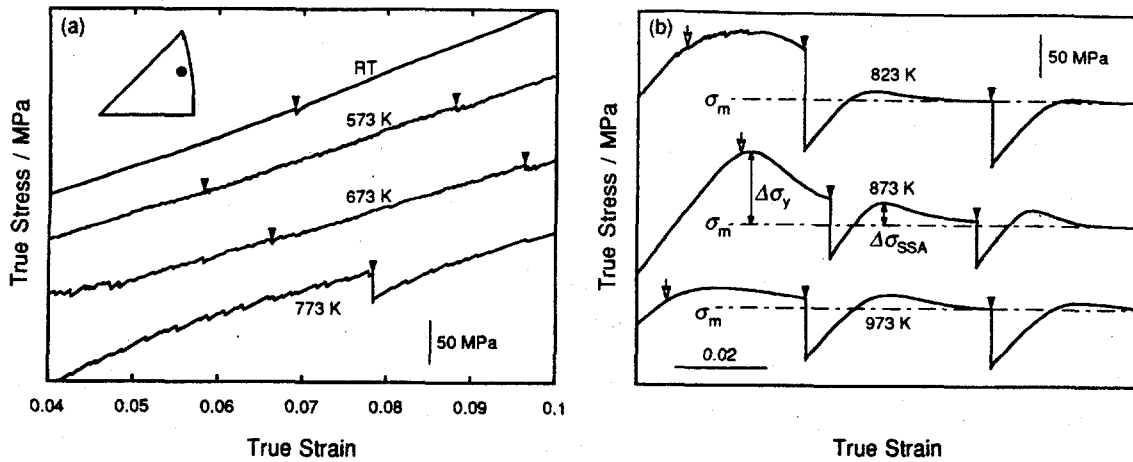
Fig. 3. Stress-strain curves of Fe-39.5Al single crystals obtained during the stress relaxation tests. Filled arrows indicate the stress relaxation points and open arrows the 0.2 % proof stress.

$\dot{\varepsilon} = 1.6 \times 10^{-4}$ s^{-1}. The relaxation time is 300 s. (a) T < Tp. (b) T ≥ Tp. Load axis is shown in (a).

relaxing, $\Delta\sigma_{SSA}$, at the temperatures. Since slip vector changes abruptly from the [111] direction to <100> directions after yielding at T_p (see a later section), such a large $\Delta\sigma_y$ may be attributed to the nucleation and multiplication of <100>-type dislocations. At higher strain or temperature, the increase in stress after relaxing would be due to SSA associated with slip in <100> directions, since the dominant operative slip direction is <100>.

Single crystals are relatively ductile [12]. We can obtain an elongation of about 17 % in vacuum at room temperature even for the near-<100> orientation. We can also obtain maximum elongation of more than 90 % at an intermediate temperature, depending on load axes. Although the elongation steadily decreases with increasing temperature beyond the maximum, the decrease in the elongation does not result from a decline in ductility, but from a local necking due to nonuniform deformation.

Orientation-dependent phenomena, and tension / compression (T/C) asymmetry

In the temperature range of the yield stress anomaly of B2 FeAl, yield stress or critical resolved shear stress (CRSS), and peak stress exhibit a characteristic orientation dependence.
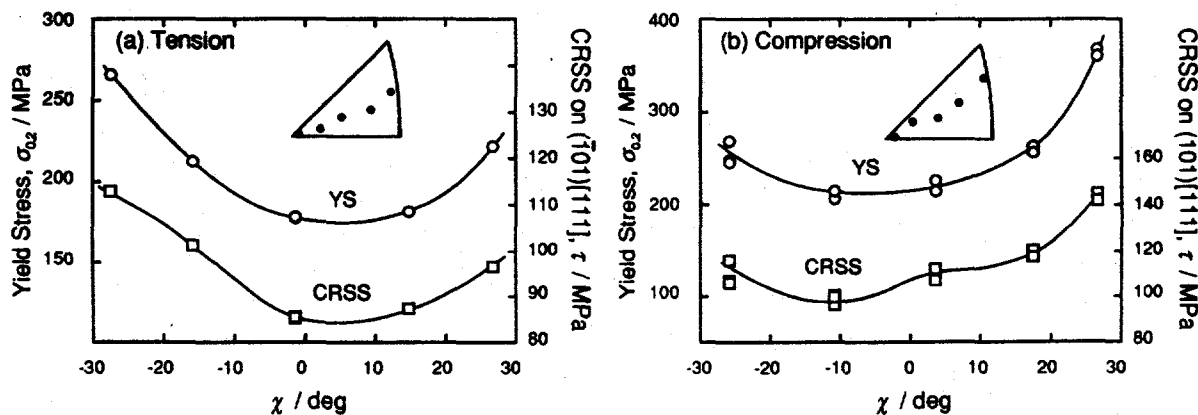

Fig. 4. χ-dependence of yield stress and critical resolved shear stress of Fe-Al single crystals at 773 K. (a) Fe-39Al in tension [12]. (b) Fe-39.5Al in compression [11].

Yoshimi et al. 3 / 12
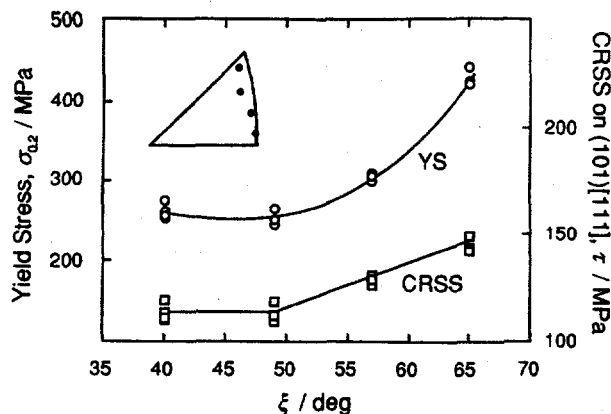
Fig. 5. ξ-dependence of yield stress and critical resolved shear stress of Fe-39.5Al single crystals at 773 K in compression [11].

Figure 4 shows orientation dependences of yield stress and CRSS at 773 K as a function of χ, where χ is the angle between the direction normal to ($\bar{1}01$) primary slip plane and that to the maximum resolved shear stress (MRSS) plane (see Ref. [11]). It should be noted that the shape of the χ-dependence is almost symmetrical between tensile and compressive straining mode, e.g., Fig. 4(a) and (b). In other words, we can express the χ-dependence in general as that yield stress and CRSS exhibit a maximum near the twinning direction and increase again near the anti-twinning direction. This tension-compression (T/C) symmetry of the χ-dependence should be a part of the intrinsic nature of deformation behavior responsible for the yield stress anomaly. This χ-dependence, however, is apparently different from that in β-CuZn obtained by Umakoshi et al. [17]. Furthermore, the yield stress and CRSS depend on ξ (Fig. 5), where ξ is the angle between the [111] direction and the load axes (also see Ref. [11]). This ξ-dependence is not in agreement with that predicted by the cross slip pinning (CSP) model.

The serrated flow behavior is also an orientation-dependent phenomenon. In tension case (Fig. 2), stress amplitude in serration is prominent for $\chi \leq 0°$, and it becomes weak or disappears with increasing χ. By contrast, in compression case, serrations were observed for the orientation of $\chi \geq 0°$, while no serration for $\chi < 0°$ [11]. Therefore, there exists a T/C symmetry also in the serrated flow behavior.

Strain-rate-dependent phenomena

Strain-rate sensitivity of yield stress of B2 FeAl single crystals is small at the strain rates examined in the temperature range of the yield stress anomaly, as shown in Fig. 6 [11]. The peak temperatures are also not so sensitive to the strain rates, but the peak stresses are remarkably sensitive. Nagpal and Baker [24] investigated the effect of strain rate on yield stress of Fe-45Al polycrystals at room temperature, and found that yield stress hardly changed with the strain rate under 10^{-2} s^{-1}. These results indicate that yield stress is hardly sensitive to strain rate in a relatively wide temperature range below T_p.

Very small strain-rate sensitivity of flow stress was confirmed by the strain-rate change tests [11]. On the other hand, in the temperature range of the yield stress anomaly, the strain-rate dependence of work hardening rate increases with increasing temperature. The work hardening rate becomes higher at a higher strain rate, indicating a normal, positive strain-rate dependence. This result on the strain-rate dependence of work hardening rate suggests that the recovery process is thermally activated in the temperature range.

The strain-rate sensitivity and the relaxation stress are plotted together as functions of temperature in Fig. 7. Within the accuracy of the recording system, I ($\equiv d\sigma/d\ln\dot{\varepsilon}$) is essentially zero up to T_p, as mentioned above. At T_p, it increases drastically and reaches a maximum. Above T_p, it exhibits a conspicuous value ($I \sim 35$ MPa) in contrast with those ($I \sim 0$ MPa) below T_p. The temperature dependence of the stress relaxation (solid curve in Fig. 7) shows a tendency
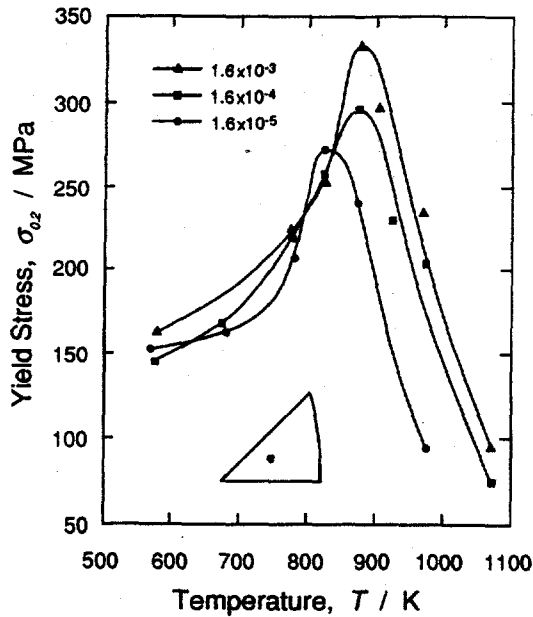
Fig. 6. Temperature dependence of yield stress of Fe-39.5Al single crystals for three strain rates [11].
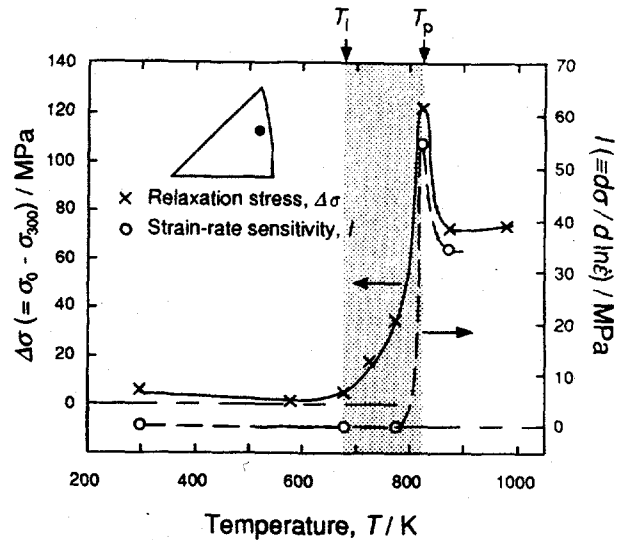

Fig. 7. Temperature dependence of the strain-rate sensitivity, I, and of the relaxation stress, $\Delta\sigma$. The strain-rate sensitivity was estimated by strain-rate changing from 1.6×10^{-4} s^{-1} to 1.6×10^{-3} s^{-1} at about 3 % plastic strain after yielding. The relaxation stress was measured by the flow stress over 300 s at about 3 % plastic strain, by stopping the cross head movement.

similar to that of the strain-rate sensitivity (dashed curve) apparently, but in the domain of the yield stress anomaly, the relaxation stress, $\Delta\sigma$, increases gradually with increasing temperature. When a recovery process takes place during the stress relaxation, the deviation from a logarithmic relaxation rate becomes large in the relaxation curve. On the other hand, a true relaxation rate ought to be as small as that below T_l in the temperature range of the anomaly, since I is almost zero. Therefore, the increase in $\Delta\sigma$ with temperature in the domain of the anomaly is attributed to an increase in a recovery rate. As the recovery process is diffusion-controlled, the rise in the recovery rate originates from enhancement in atomic diffusivity. Accordingly, we can expect that deformation above T_l is controlled by a diffusion-assisted process of dislocation motion.

SLIP TRANSITION AND DEFORMATION MICROSTRUCTURE

Umakoshi and Yamaguchi first reported that slip direction changes from <111> at lower temperature to <100> at higher temperature [25, 26]. A similar slip transition has been reported also in Fe$_3$Al [27] and β-CuZn [28, 29]. In β-CuZn, Saka and his colleagues observed that the fraction of densities of <111>-type and non-<111>-type dislocations drastically changes around T_p [28, 29]. The reason why the yield stress anomaly was not observed in the reports by Umakoshi and Yamaguchi [25, 26] is probably due to the excess vacancy strengthening that might have obscured it [6, 14]. Till recently, a relationship between the yield stress anomaly and the slip transition had not been well established in B2 FeAl.

Slip directions determined by the two-surface trace analysis are shown in Fig. 1. It should be noted that the macroscopic slip transition temperatures coincide with the peak temperatures. Accordingly, the decline in yield stress above T_p, was attributed to a negative temperature dependence of CRSS for the slip in non-<111> directions.

As shown in Fig. 8, at T_p, a deforming crystal exhibits serrated flow, and slip is very inhomogeneous within some initial strain (curves a and b). As shown in the inserted photograph a of Fig. 8, only a few coarse slip bands parallel to ($\bar{1}01$) plane appear on the surface of a specimen strained to a near-yield strain of 0.5 %. With increasing strain, the slip bands propagated over the specimen. Beyond the certain strain (~2 %), serrations disappear and instead remarkable work-softening occurs (curve c). A surface of the specimen corresponding to the curve c is shown in the inserted photograph c. As slip bands propagated throughout the entire specimen, slip traces other than the ($\bar{1}01$) planes were also detected on the surface. Thus, it can be expected that dislocation structures in the specimen a, b and c would be all very different.

Dislocation structure within a coarse slip band of the specimen a is shown in Fig. 9. Almost all the dislocations were confirmed to be of [111]-type by using conventional $\mathbf{g} \cdot \mathbf{b} = 0$ invisibility criteria under several $\mathbf{g}$ vectors. Hence, it was revealed that <111> slip is predominantly activated at the early stage of plastic deformation even at T_p. This result also confirms that the yield stress anomaly is caused by the increase in the glide resistance to <111>-type superdislocations.

Figure 10 shows bright-field micrographs of dislocation structure of specimen b in Fig. 8, which was strained before work-softening. Interestingly, most of the dislocations are out of contrast or in weak residual contrast under $\mathbf{g} = 020$ (Fig. 10(a)), while others exhibit a weak, dotted contrast under $\mathbf{g} = 101$ (Fig. 10(b)). These results of the contrast analysis indicate that those dislocations are of non-[111], i.e., <100> or <110>-type. We deduce from this evidence
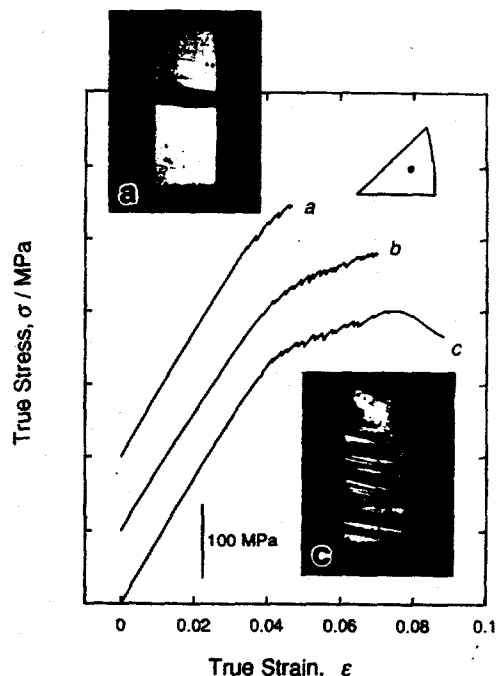

Fig. 8. Stress-strain curves of Fe-39.5Al single crystals deformed to three different strains at 823 K ($\approx T_p$).

Fig. 9. Bright field micrograph taken in a slip band of specimen a. B $\cong$ [$\bar{1}01$]. $\mathbf{g} = 101$.
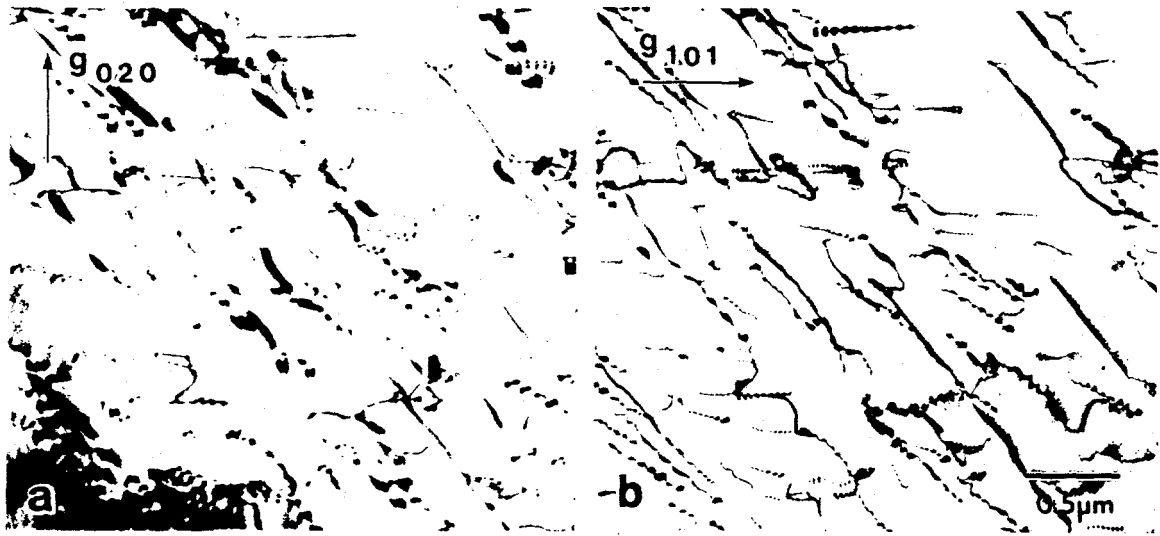
Yoshimi et al.   6 / 12

Fig. 10. Bright field micrographs taken in specimen b. $B \cong [\bar{1}01]$. (a) $g = 020$. (b) $g = 101$.

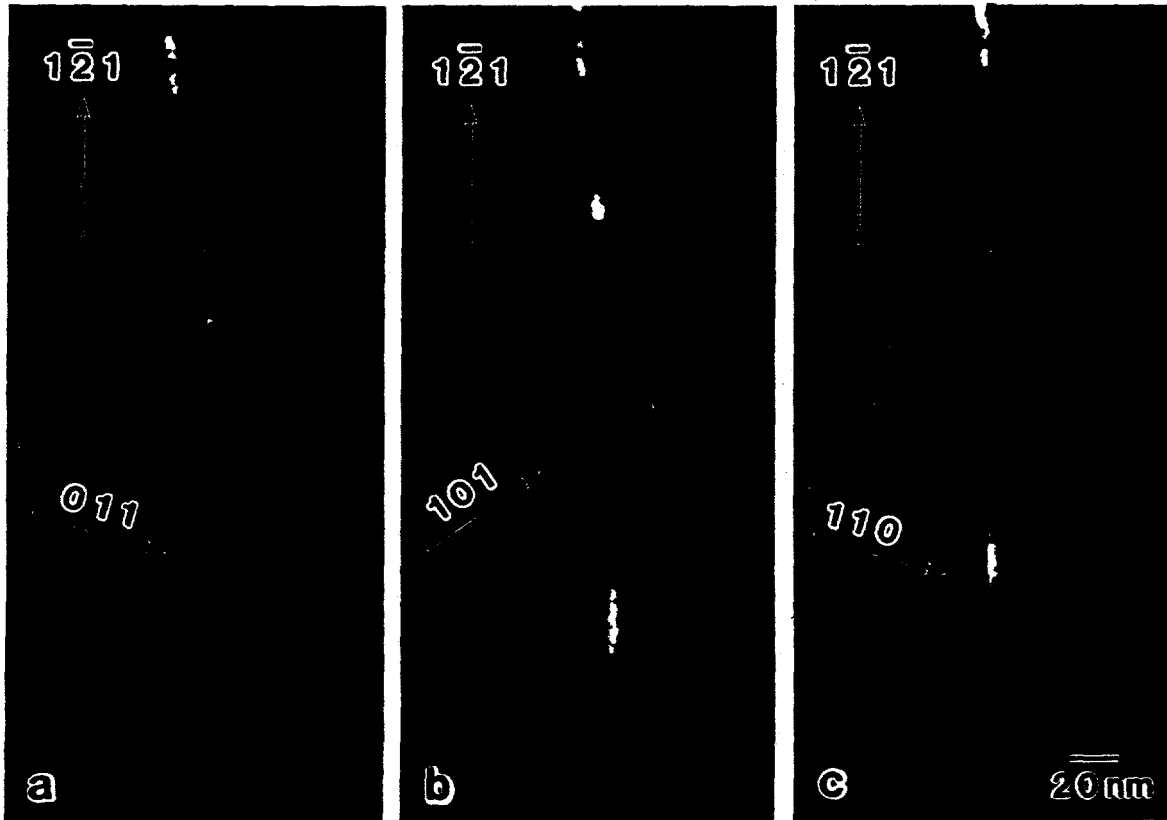

Fig. 11. Weak-beam micrographs upon tilting around the $[1\bar{2}1]$ direction in the same foil as in Fig. 9 under $g - 4g$ condition. (a) $B \cong [\bar{3}\bar{1}1]$. $g = 011$. (b) $B \cong [\bar{1}01]$. $g = 101$. (c) $B \cong [\bar{1}13]$. $g = 110$.

that slip direction changes during deformation with increasing strain. In the specimen c, almost all dislocations were of <100>-type, suggesting that the slip transition had been already completed at this strain.

Figure 11 shows weak-beam micrographs taken by the tilting experiment using the $[1\bar{2}1]$ axis in the same foil as in Fig. 9. It can be seen that the near-edge segment is not dissociated into superpartials from the direction normal to the macroscopic slip plane, i.e., the $(\bar{1}01)$ plane (Fig. 11 (b)). On the other hand, it is found to partly dissociate into superpartials from the $[3\bar{1}1]$ and the $[\bar{1}13]$ directions, which are apart by 30° around the $[1\bar{2}1]$ axis. Those dislocation pairs are not dipoles, but consist of superpartials, indicating that those <111>-type superdislocations are climb-dissociated. Such a climb dissociation was often observed in the specimens deformed in the domain of the anomaly. From these observations, we conjecture that the climb dissociation may generate locking stress in the temperature range of the anomaly. However, we cannot observe the arrangement of <111>-type superdislocations preferentially along a specific orientation, such as edge or screw direction at the peak temperature (Fig. 9), which is different from the microstructure observed in some $L1_2$ intermetallic compounds [e.g. 30 - 33]. These "feature-less" deformation microstructures of mixed dislocation characters in the domain of the yield stress anomaly prevent us from ascertaining the pinning mechanisms for <111>-type superdislocations.

DISCUSSION

The results shown in Figs. 8 and 9 confirm that yield stress anomaly of B2 FeAl is induced by the increase in the glide resistance to <111>-type superdislocations with increasing temperature. In our early work [10], we observed the decomposed configuration of [111]-type dislocations into [010]-type and [101]-type ones in the specimen deformed just below T_p. However, decomposition was hardly observed in the specimen deformed at T_p in spite of a still significant <111> slip activity (Fig. 9). This means that such decomposition is not a major cause for the yield stress anomaly.

As shown in Figs. 8 - 10, it was found that the slip direction changed from <111> to <100> during deformation with increasing strain at T_p. This suggests that the decomposition may still occur during work hardening and it may become the primary source for <100>-type dislocations. Indeed, the density of <111>-type dislocations is much lower after the transition (Fig. 10) than before it (Fig. 9). If the source of <100>-type dislocations was activated independently from decomposition, there would be more <111>-type dislocations left in the specimen.

Since the yield stress above T_p is controlled by CRSS of <100> slip, T_p is determined as the intersection between the yield stress curves for the <111> slip and that for the <100> slip. Peak temperatures in the Fe-Al system reported by many researchers [1 - 8, 10 - 15, 20, 21, 27, 33 - 36] are summarized in Fig. 12. At the aluminum content less than about 30 %, where alloys are undoubtedly of the DO_3-ordered state at room temperature, the data of the peak temperatures are located around 800 K with a small scatter. On the other hand, at aluminum contents greater than 30 %, the observed peak temperatures are much more scattered. As one of possible causes for the good reproducibility of the peak temperatures at lower aluminum contents, we can recognize the role of the first-order phase transformation (DO_3 / ($DO_3 + \alpha$)) and the second-order one (DO_3 / B2). Some results indicate that peak temperatures lie above the transformation temperatures [21, 35]. This evidence suggests that the phase transformations are not a *direct*
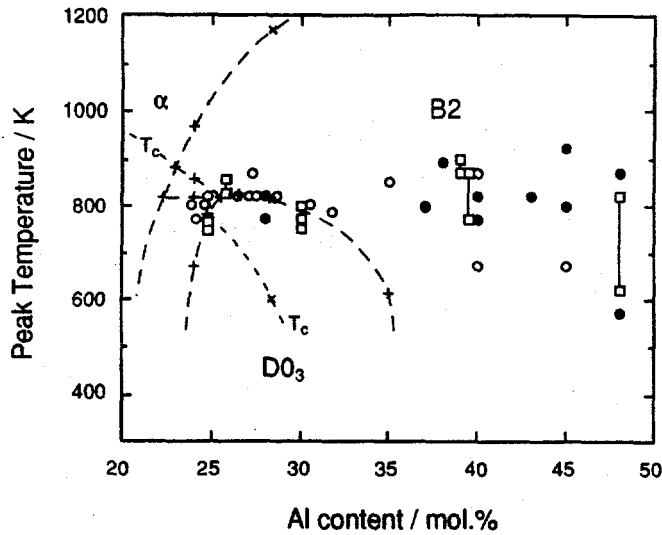
Fig. 12 Peak temperature reported in Refs. [1-8, 10-15, 20, 21,27, 33-36] as a function of Al content. Open circles indicate binary polycrystals, filled ones polycrystals modified by added elements, and open squares binary single crystals. Broken lines indicate the phase transformation temperature reported in Refs [22, 53].

source for the increase in yield stress. Furthermore, the peak temperatures do not correspond to the transformation temperatures at higher aluminum contents. Thus, it is reasonable to seek a common strengthening mechanism other than the phase transformations operating on <111>-type superdislocations in the wide composition range irrespective of ordered states.

The local climb locking [9] is one of the most convincing locking mechanisms for the yield stress anomaly observed in B2 FeAl. According to Flinn's calculation [37], APB energies for B2-ordered structure are ranked as {001} > {112} > {110} > {111}. If this calculation is correct, it is expected that the climb-dissociated configuration is energetically preferable to the glide-dissociated one for <111>-type superdislocations, since the {111} plane is the climb plane for the edge character. This energetic preference induced by the anisotropy of APB energy would offer specific driving force for the climb dissociation of edge dislocations. Thermal formation of APBs on {111} planes (Fig. 13) has been reported in Fe-Al containing more than 35%Al [38 - 41]. Yoshimi et al. [41] interpreted the APB formation as a result of collapse of the lattice owing to vacancy condensation on triple layers of {111} planes during a heat treatment at an intermediate temperature. Such APB formation indicates that APB energy is estimated to be lower on the
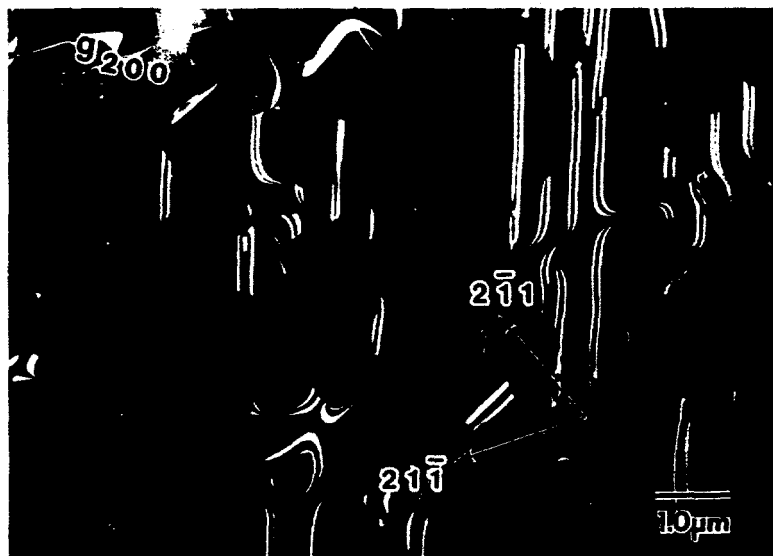

Fig. 13. A typical APB structure formed by vacancy condensation in Fe-35Al [41].

{111} plane than on the {110} plane even at the elevated temperature. This result strongly supports the result calculated by Flinn [37]. Moreover, Marcinkowski and Brown [42] calculated NN- and NNN-APB energies in DO_3 Fe_3Al in the similar manner to Flinn's, where NN-APB is the APB introduced by $\frac{1}{4}a_0'<111>$ shear displacement in the DO_3 lattice, NNN-APB by $\frac{1}{2}a_0'<111>$ or $\frac{1}{2}a_0'<100>$ shear displacement, and a_0' the lattice parameter of DO_3 Fe_3Al. According to their calculation [42], the NN-APB energy exhibits the anisotropy similar to that in B2 compounds calculated by Flinn, while the NNN-APB energy exhibits the anisotropy opposite to NN-APB energy and that in B2 compounds. The anisotropy of the APB energies in DO_3 Fe_3Al has been also supported by the observation by Mendiratta et al. [43]. Thus, it can be expected that specific driving force for climb dissociation also exists between superpartials connected by NN-APB in Fe_3Al. This interpretation is in good agreement with a TEM result observed by Morris et al. [27]. In addition, it is worth noting that the superpartial pairs connected by NN-APB are equivalent to superpartial pairs in B2 FeAl. Consequently, we can consider that the driving force for the climb dissociation results from the same origin for both DO_3 Fe_3Al and B2 FeAl. Climb-dissociation of superdislocations in B2 compounds has been investigated for the yield stress anomaly in β-CuZn by Saka and Zhu [44], Zhu and Saka [45] and Dirras et al. [46]. However, Dirras et al. [46] denied that the anomaly results only from the climb dissociation.

Frictional stress due to APB dragging would be another that may give rise to the glide resistance on $<111>$-type superdislocations. In Brown's original idea [47], the frictional stress is proportional to temperature and square of long range order parameter, and inverse to Burgers vector. Applying this concept to B2 FeAl having the composition more than 35%Al as an example, the frictional stress must increase with increasing Al content at an elevated temperature. Because the fraction of Al-sites occupied by Fe atoms decreases, i.e., the long range order state rises with increasing Al content [48 - 50], which is hardly reduced up to a high temperature above T_p [22], although the lattice parameter is almost constant in this composition range [51]. We have, unfortunately, no available data for this discussion at present, because yield stress in the domain of the anomaly is drastically changed by impurity level, crystal orientation, heat treatment, microstructure, and so on, as shown in Fig. 12. Beauchamp et al. [52] investigated the structure of the APB on {110} plane in β-CuZn using CVM and attempted to explain yield stress anomaly of β-CuZn on the basis of APB dragging mechanism. The barrier against dislocation motion adopted in their model is the atomic rearrangement at APB. They pointed out that the strengthening caused by both APB rearrangement and the climb dissociation belongs to the same family of phenomena. Although their prediction for T_1 and T_p is apparently in agreement with our results observed in FeAl single crystals, it still leaves us with difficulty to expand their model over Fe-Al system.

SUMMARY

In our study by using B2 FeAl single crystals, it was confirmed that $<111>$ slip is activated predominantly at the early stage of plastic deformation even at T_p. This observation indicates that the yield stress anomaly is caused by the increase in the glide resistance against $<111>$-type superdislocations. Also, it has been revealed that the temperature domain of the anomaly is that a thermally-activated recovery process is gradually enhanced with increasing temperature out of the regime of low temperature deformation mode with no diffusional assist. In addition, work hardening exhibits a normal, positive strain rate sensitivity in the temperature range. Accordingly, we can expect that deformation in the temperature domain of the anomaly is controlled by a

diffusion-assisted process of dislocation motion such as climb dissociation and/or APB dragging. The APB formation on {111} plane by vacancy condensation indicates that APB energy on {111} plane is lower than that on {110} plane. This anisotropy of APB energy would generate energetically stable core configuration for climb dissociated edge dislocations. However, we could not observe the arrangement of <111>-type superdislocations preferentially along the edge orientation in the domain of the anomaly. These feature less dislocation microstructures are the ones keeping us from conclusively determining the pinning sites on <111>-type dislocations.

We still leave several unsolved problems for understanding the yield stress anomaly of B2 FeAl. For examples, very small strain rate sensitivity, orientation dependence and T/C asymmetry of yield stress and serration flow, effect of work hardening at micro strains, and so on. In order to solve the above problems, further basic researches by means of precise experiments using single crystals are needed.

ACKNOWLEDGMENT

REFERENCE

1. I. Baker and D. J. Gaydosh, Mater. Sci. Eng., **96**, 147 (1987).
2. J. T. Guo, C. Sun, M. H. Tan, H. Li and W. H. Lai, Acta Metall.Sinica A, **3**, 249 (1990).
3. K. -M. Chang, Metall. Trans. A, **21A**, 3027 (1990).
4. H. Xiao and I. Baker, Scripta Metall. Mater., **28**, 1411 (1993).
5. J. T. Guo, O. Jin, W. M. Yin and T. M. Wang, Scripta Metall. Mater., **29**, 783 (1993).
6. K. Yoshimi, S. Hanada and H. Tokuno, Mater. Trans. JIM, **35**, 51 (1994).
7. O. Klein and I. Baker, Scripta Metall. Mater., **30**, 1413 (1994).
8. T. Onuma, M. S. Thesis, (Tohoku University, 1995).
9. D. G. Morris, Phil. Mag. A, **71**, 1281 (1995).
10. K. Yoshimi and S. Hanada, in Structural Intermetallics, ed. by R. Darolia, J. J. Lewandowski, C. T. Liu, P. L. Martin, D. B. Miracle and M. V. Nathal, (TMS, Warrendale, PA, 1993), p. 475.
11. K. Yoshimi, S. Hanada and M. H. Yoo, Acta Metall. Mater., **43**, 4141 (1995).
12. K. Yoshimi, S. Hanada and M. H. Yoo, Intermetallics, **4**, 159 (1996).
13. N. Matsumoto, M. S. Thesis, (Tohoku University, 1994).
14. R. Carleton, E. P. George and R. H. Zee, Intermetallics, **3**, 433 (1995).
15. K. Yoshimi, S. Hanada and M. H. Yoo, Intermetallics, **4**, S159 (1996).
16. G. W. Ardley and A. H. Cottrell, Proc. Roy. Soc., **219**, 328 (1953).
17. Y. Umakoshi, M. Yamaguchi, Y. Namba and K. Murakami, Acta Metall., **24**, 89 (1976).
18. A. Nohara, M. Izumi, H. Saka and T. Imura, Phys. Stat. Sol. (a), **82**, 163 (1984).
19. A. Lawley, E. A. Vidoz and R. W. Cahn, Acta Metall., **9**, 287 (1961).
20. N. S. Stoloff and R. G. Davies, Acta Metall., **12**, 473 (1964).
21. S. Hanada, S. Watanabe, T. Sato and O. Izumi, Scripta Metall., **15**, 1345 (1981).
22. G. Inden and W. Pepperhoff, Z. Metallkde., **81**, 770 (1990).
23. D. G. Morris, J. C. Joye and M. Leboeuf, Phil. Mag. A, **69**, 961 (1994).
24. P. Nagpal and I. Baker, Scripta Metall. Mater., **25**, 2577 (1991).
25. Y. Umakoshi and M. Yamaguchi, Phil. Mag. A, **41**, 573 (1980).

26. Y. Umakoshi and M. Yamaguchi, Phil. Mag. A, **44**, 711 (1981).
27. D. G. Morris, D. Peguiron and M. Nazmy, Phil. Mag. A, **71**, 441 (1995).
28. H. Saka and M. Kawase, Phil. Mag. A, **49**, 525 (1984).
29. A. Matsumoto and H. Saka, Phil. Mag. A, **67**, 217 (1993).
30. B. H. Kear and H. G. F. Wilsdorf, Trans. TMS-AIME, **224**, 382 (1962).
31. P. H. Thornton, R. G. Davies and T. L. Johnston, Metall. Trans., **1**, 207 (1970).
32. S. Takeuchi and E. Kuramoto, Acta Metall., **21**, 415 (1973).
33. P. Morgand, P. Mouturat and G. Sainfort, Acta Metall., **16**, 867 (1968).
34. W. Schröer, H. Mecking and Ch. Hartig, in <u>Intermetallic Compounds</u>, ed. by O. Izumi, (JIM, Sendai, Japan, 1991), p. 567.
35. J. W. Park, I. G. Moon and J. Yu, J. Mater. Sci, **26**, 3062 (1991).
36. H. Rösner, G. Molenat, M. Kolbe and E. Nembach, Mater. Sci. Eng., **A192/193**, 793 (1995).
37. P. A. Flinn, Trans. TMS-AIME, **218**, 145 (1960).
38. D. Weber, M. Meurtin, D. Paris, A. Fourdeux and P. Lesbats, J. Phys. C7, **38**, 332 (1977).
39. N. Junqua, J. C. Desoyer and P. Moine, Phys. Stat. Sol. (a), **18**, 387 (1973).
40. A. Fourdeux and P. Lesbats, Phil. Mag. A, **45**, 81 (1982).
41. K. Yoshimi, S. Hanada, T. Onuma and M. H. Yoo, Phil. Mag. A, **73**, 443 (1996).
42. M. J. Marcinkowski and N. Brown, J. Appl. Phys., **33**, 537 (1962).
43. M. G. Mendiratta, S. K. Ehlers and H. A. Lipsitt, Metall. Trans. A, **18A**, 509 (1987).
44. H. Saka and Y. M. Zhu, Phil. Mag. A, **51**, 629 (1985).
45. Y. M. Zhu and H. Saka, Phil. Mag. A, **59**, 661 (1989).
46. G. Dirras, P. Beauchamp and P. Veyssiére, Phil. Mag. A, **65**, 815 (1992).
47. N. Brown, Phil. Mag., **4**, 693 (1959).
48. A. J. Bradley and A. H. Jay, Proc. Roy. Soc. A, **136**, 210 (1932).
49. A. Lawley and R. W. Chan, J. Phys. Chem. Solids., **20**, 204 (1961).
50. T. Eguchi, H. Matsuda, K. Oki, S. Kiyoto and K. Yasutake, Trans. JIM, **8**, 174 (1967).
51. H. J. Leamy, E. D. Gibson and F. X. Kayser, Acta Metall., **15**, 1827 (1967).
52. P. Beauchamp, G. Dirras and P. Veyssiére, Phil. Mag. A, **65**, 477 (1992).
53. W. Köster and T. Gödecke, Z. Metallkde., **71**, 765 (1980).

DISCLAIMER

Yoshimi et al. 12/12